Bryce Arthur Martin Marchick, 1250084[1,*]

[1]*Department of Physics, University of Alberta, Edmonton, AB, Canada T6G 2G7*

This paper is a review of CERN's "Observation of a new particle in the search for the Standard Model Higgs boson with the ATLAS detector at the LHC". It breaks down the CERN paper so that a fourth year physics student will be able to understand it.

I. INTRODUCTION

The Standard Model (SM) of particle physics describes the interactions of subatomic particles. It catalogs the elementary particles, the leptons and quarks, and describes how the four fundamental forces interact with the particles. All particles in the SM have been observed experimentally, with the final particle, the Higgs boson, being only recently observed. The Higgs boson gives mass to massive elementary particles, and is a scalar particle (spin 0).

The goal at CERN was to measure the mass of the Higgs boson. This was done by colliding hadrons (protons in this case) with a total energy of 8 TeV in the Large Hadron Collider (LHC) and use the ATLAS detector to measure the resulting collisions. The Higgs boson has several possible measurable decays: $H \to \mathrm{ZZ}^{(*)} \to 4$, $H \to \gamma\gamma$, and $H \to \mathrm{WW}^{(*)} \to e\nu_e\mu\nu_\mu$.

Previously, in 2011, the LHC determined a mass in the vicinity of 124-126 GeV with a significance of 2.9 and 3.1 standard deviations (σ) respectively, using an average collision energy of 7 TeV [1]. A significance of 5 σ is required for CERN to declare a discovery.

Therefore, in 2012, CERN increased the collision energy to 8 TeV in order to improve particle detection, identification and reconstruction of the collisions [1]. The $e\nu_e$ channel provided most of the sensitivity of the search, so only this final state was used in the analysis of the 8 TeV data since the $e\mu$ endstate restricts the channel possibilities and is therefore easier to use in analysis.

II. DETECTION

A. The ATLAS Detector

The ATLAS detector (Fig 1) consists of 4 main components: the Inner Detector (ID), the calorimeter, the magnet system and the muon spectrometer (MS).

The ID measures the momentum of each charged particle. It combines high-resolution detectors at the inner radii with continuous tracking elements at the outer radii, all contained in the Central Solenoid, which provides a nominal field of 2 T. [2]

The calorimeter measures the energies of charged and neutral particles. It is divided into a central barrel $|\eta| <$ 1.475, an outer end cap $1.375 < |\eta| < 2.5$ and an inner end cap $2.5 < |\eta| < 3.2$ (see section XI A. Pseudorapidity for details). It consists of metal plates (absorbers) and sensing elements. Interactions in the absorbers transform the incident energy into a "shower" of particles that are detected by the sensing elements. In the inner sections of the calorimeter, the sensing element is liquid argon. The showers in the argon liberate electrons that are collected and recorded. In the outer sections, the sensors are tiles of scintillating plastic. The showers cause the plastic to emit light which is detected and recorded. [2]

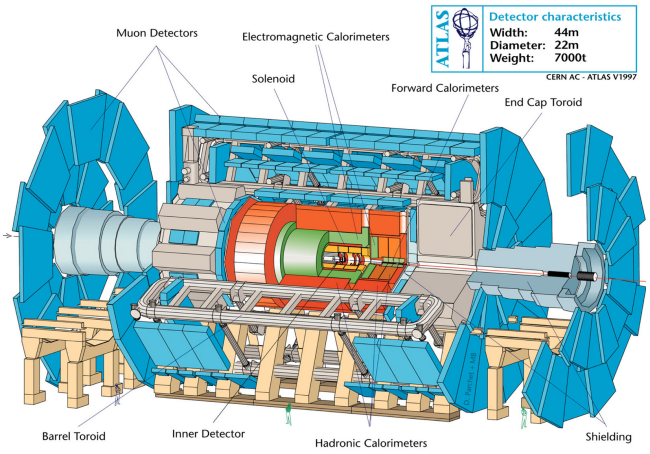

FIG. 1: Cut-away view of the ATLAS detector. The dimensions of the detector are 25 m in height and 44 m in length.

The magnet system is comprised of the Solenoid Magnet (SM) and the Toroid Magnets (TM), which bend charged particles for momentum measurements. The central SM is a composite that consists of a flat superconducting cable located in the center of an aluminum stabilizer with rectangular cross-section. It is designed to provide a field of 2 T with a peak magnetic field of 2.6 T. The TM system consists of eight Barrel coils housed in separate cryostats and two End-Cap cryostats housing eight coils each. The End-Cap coils systems are rotated by 22.5° with respect to the Barrel Toroids in order to provide radial overlap and to optimize the bending power in the interface regions of both coil systems. [2]

The MS surrounds the calorimeter and measures muon paths to determine their momenta with high precision. The muons are the only detectable particles that can traverse all the calorimeter absorbers without being stopped. The detector consists of thousands of charged particle sensors placed in the magnetic field produced by TM. [2]

*Electronic address: marchick@ualberta.ca

Process	Event Generator Program
ggF, VBF	PYTHIA and POWHEG
$WH, ZH, t\bar{t}H$	PYTHIA
$q\bar{q}/gg \to \gamma\gamma$	SHERPA

TABLE I: Event generators used in search for Higgs boson. PYTHIA indicates PYTHIA6 and PYTHIA 8 are used for the 7 TeV and 8 TeV data respectively.

B. Data Filtering and Event Selection

The interactions in the ATLAS detectors will create many events and decays. The majority of these are not needed as only a small handful of results are interesting. In order to sift through the junk data, several methods are used: the trigger system, the data acquisition system and the event selector.

The first-level (LVL1) trigger works on a subset of information from the calorimeter and muon detectors. All of the information from the detector must be stored in memory until the LVL1 decision is available. The data can be accessed selectively by the LVL2 trigger which uses regions of interest defined by the LVL1 trigger. The LVL2 trigger refines the selection of candidate objects compared to LVL1, using information from all detectors, including the inner tracker which is not used at LVL1. Many events are analyzed concurrently by the LVL2 trigger system using processor farms. For interesting data selected by LVL2, event reconstruction is performed. [1, 2]

III. SIGNAL AND BACKGROUND SIMULATION SAMPLES

The SM Higgs boson production processes considered in the analysis are the dominant gluon fusion (ggF) $gg \to H$, vector-boson fusion (VBF, $qq' \to qq'H$) and Higgs-strahlung (WH/HZ, $qq' \to WH, ZH$). For the photon pair production process (pp) $H \to \gamma\gamma$, only the small contribution from the associated $t\bar{t}$ pair interaction ($t\bar{t}H$, $q\bar{q}/gg \to t\bar{t}H$) is taken into account for the pp process.[1]

The total cross sections (see section XI B. Cross Section) for SM Higgs boson production at the LHC with $M_h = 125$ GeV are predicted to be 17.5 pb for $\sqrt{s} = 7$ TeV and 22.3pb for $\sqrt{s} = 8$ TeV. [1]

The branching ratios (see section XI C. Branching Ratio) of the SM Higgs boson as a function of m_h are calculated using programs.

Table. I displays the relevant programs used to model the signal and background processes.

IV. THE $H \to ZZ^{(*)} \to 4l$ CHANNEL

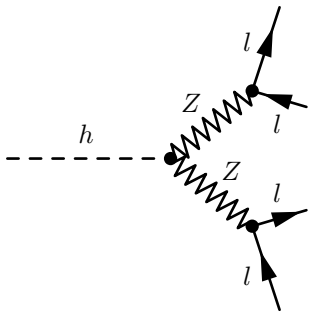

This channel provides good sensitivity over a large mass range (110-600 Gev) due to the high momentum resolution of the ATLAS detector. [1]. This analysis searches for Higgs boson candidates by selecting two pairs of isolated leptons, each of which is comprised of two leptons with the same flavour but opposite charge. The two leptons could be electrons and/or muons, with their corresponding neutrino.

The expected cross section times branching ratio for this channel is 2.2 fb for $\sqrt{s}$ =7 TeV and 2.8 fb for $\sqrt{s}$ =8 TeV.[1]

A. Event Selection

The data are selected using single-lepton or dilepton triggers. Muon candidates are formed by matching reconstructed ID tracks with either a complete track or a track-segment reconstructed in the MS. Electron candidates must have a well-reconstructed ID track pointing to an electro-magnetic calorimeter cluster and the cluster should satisfy a set of identification criteria. These profiles are fitted using a Gaussian-Sum Filter which allows for bremsstrahlung energy losses to be taken into account. [1]

The algorithm suppresses noise by keeping tracks with a significant energy compared to tracks farther away. Corrections for bremmstrahlung and electron-electron interactions is also done at this point.

B. Background Estimation

A Monte Carlo (MC) method is used to estimate background yield and composition. The MC method relies on repeated random sampling to obtain numerical results. For systems with many coupled degrees of freedom, complicated boundary conditions and significant uncertainty, the MC method is used to evaluate multivariable integrals. In elementary particle physics, the phase space is known. Theoretical functions are used as a weight to a random number generator (RNG) to generate events. Once a MC event sample is generated, it is normalized to the theoretical cross section for $ZZ^{(*)}$ production, and can be used "as data" [1, 3]. MC events were generated

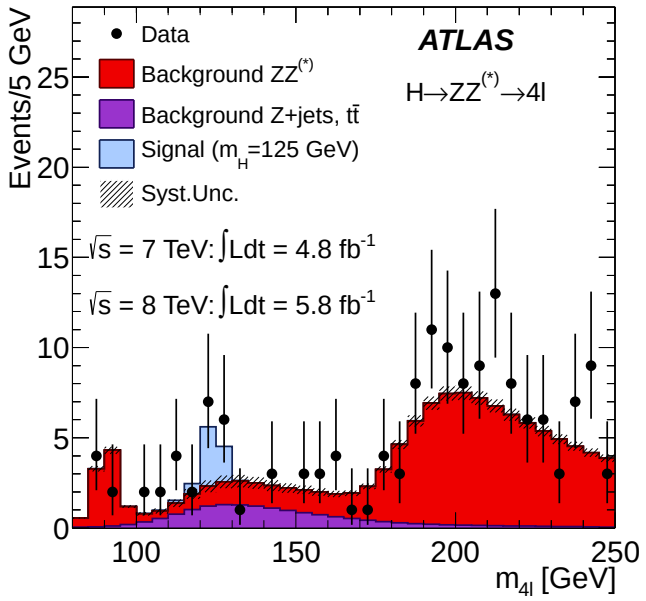

FIG. 2: Distribution of the four-lepton invariant mass for the selected candidates compred to background expectations for the combination of the 7 TeV and 8 TeV data.

before the real data, according to the detector limitations and to the theoretical expectations from the SM. The existence of these MC data sets allowed fast checks on whether new physics is appearing. New physics will appear as statistically significant deviations from the Monte Carlo curves. [3]

C. Systematic Uncertainties

The uncertainties on the integrated luminosities (see section XI D. Luminosity for details) are determined to be 1.8% for the 7 TeV data and 3.6% for the 8 TeV data using several luminosity-sensitive detectors For cross-section measurements, the uncertainty on the delivered luminosity is often one of the dominant systematic uncertainties. [1]

The uncertainties on the lepton reconstruction and identities are done using samples of W, Z and J/Ψ decays done in the 2011 data.[1]

For the SM $ZZ^{(*)}$, which is estimated from MC simulation, the uncertainty on the total yield due to QCD scale uncertainty is $\pm 5\%$ while the effect of the PDF and α_s uncertainties is $\pm 4\%$ for processes initialted by quarks or gluons. The impact of not using the theoretical constraints on the $ZZ^{(*)}$ yield has been found to be negligible.[1]

D. Results

Fig 2 shows the mass distribution for the four leptons (two pairs of electrons, or two pairs of muons, or the pair of electrons and the pair of muons). Accounting also for the decay angle characteristics, it yields an excess of 3.2 sigma above background at a mass near 125 GeV.[1]

V. THE $H \to \gamma\gamma$ CHANNEL

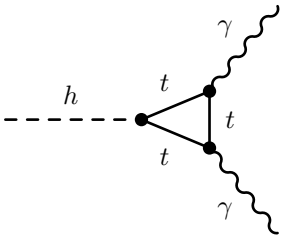

The search for the SM Higgs through the decay $H \to \gamma\gamma$ is performed in the mass range of 110 GeV to 150 GeV. Background contributions are $\gamma+$ jet and jet + jet production. Higgs boson events produced by VBF processes have two forward jets, originating from the two scattered quarks, and tend to be devoid of jets in the central axis region.

A. Event Detection

The data used in this channel are selected using a diphoton trigger, which requires two clusters formed from energy depositions in the electromagnetic calorimeter. Data selection is refined by placing threshold values on the transverse energy, which in effect limits the mass range search of the Higgs boson. Shapes of the clusters are also evaluated to match expectations for electromagnetic showers initiated by photons. In total, this gives a 99% trigger efficiency for events passing the final event selection.[1]

In order to account for energy losses outside of the cluster, MC simulation results are used to calibrate the energies of the photon candidates. The calibration is defined by applying η-dependent correction factors, which are on the order of $\pm 1\%$, determined from measured $Z \to e^+e^-$ events. [1]

Photon candidates are required to pass identification criteria based on shower shapes in electromagnetic calorimeter and on energy leakage into the hadronic calorimeter.[1]

B. Invariant Mass Reconstruction

The invariant mass of the photon is evaluated using the photon energies measured in the calorimeter, the azimuthal angle ϕ between the photons as determined from

the positions of the photons in the calorimeter, and the values of η calculated from the positions of the identified primary vertex and the impact points of the photons in the calorimeter. The primary vertex of the interaction is identified by combining the following information in a global likelihood: the directions of the photons as determined by the electromagnetic calorimeter, the parameters of the beam spot and the sum of the transverse momenta of the tracks associated with each reconstructed vertex. The tracking information from the ID improves the identification of the vertex of the interaction, which is needed for the jet selection.[1]

C. Event Categorization

The events are separated into ten different categories depending on their mass resolution and background noise. This is done to increase sensitivity and pick out Higgs boson signals. One category is only for events containing two jets, as this corresponds to VBF. The other categories make distinctions between photons that would not have come from a Higgs, photons likely to have originated from a Higgs, central photons , transition photons ($1.3 < |\eta| < 1.75$) and all others. These are then further divided depending on their transverse momentum. MC studies show that signal events, particularly those produced via VBF or associated production (WH/ZH and $t\bar{t}H$) have, on average, larger transverse momentum than background events. [1]

D. Background Modeling

The background for each event category is estimated from the data by fitting the Higgs mass range (100-160 GeV) to a selected model with free parameters for shape and normalization. The models are chosen to achieve a good compromise between limiting the size of a potential bias while retaining good statistical power[1]. A fourth-order Bernstein polynomial function is used for low transverse momentum "other" categories, and an exponential function of a second order polynomial for the central and transition categories and an exponential function for all others. [1]

Bias is handled by using large samples of simulated background events along with data-driven estimates. The background shapes are cross checked with data from control tests. The potential bias for each model is estimated separately for each category by performing a maximum likelihood fit to large samples of simulated background events in the mass range $100 - 160$ GeV. The signal shape is then taken to follow expectations for a SM Higgs boson, meaning the signal yield is a free parameter of the fit. The potential bias is then defined by the largest absolute signal yield obtained from the likelihood fit to the simulated background samples for a hypothesized Higgs boson mass in the range 110-150 GeV.

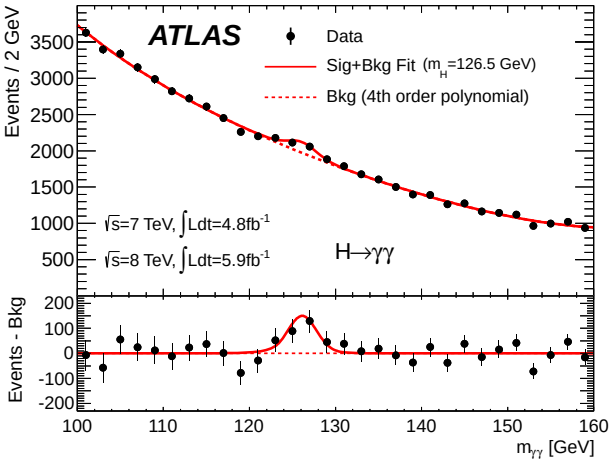

FIG. 3: Invariant mass distribution of diphoton candidates for the combined $\sqrt{s} = 7$ TeV and root $\sqrt{s}$ 8 TeV data samples. The result of a fit to the data of the sum of a signal component fixed to mH = 126.5GeV and a background component described by a fourth-order Bernstein polynomial is superimposed.

[1]

E. Systematic Uncertainties

The dominant uncertainty comes from photon reconstruction, which is due to the energy resolution of the calorimeter as it can only reconstruct photons using electrons from Z decays and photons from $Z \to l^+l\_\gamma$ events. This amounts to $\pm 8\%$ for the 7 TeV data and $\pm 11\%$ for the 8 TeV data. Luminosity uncertainty amounts to $\pm 1.5\%$ and $\pm 3.6\%$ for the 7 and 8 TeV data.

The total uncertainty on the mass resolution is $\pm 14\%$, after taking all other uncertainties (cross section, production modeling, pile-up modeling, etc).

F. Results

The $\gamma\gamma$ mass distribution is shown in Fig 3. There is an excess of events above background with a significance of 4.1 sigma, at a mass near 125 GeV. The observation of the two-photon final state implies that the new particle is a boson, not a fermion, and that it cannot be a spin 1 particle. [1]

Note that the fit is "higher" at higher energies as this is above the threshold value for Higgs production. Therefore, there are still some Higgs bosons being produced at these higher energies.

VI. THE $H \to WW^* \to e\nu_e\mu\nu_\mu$ CHANNEL

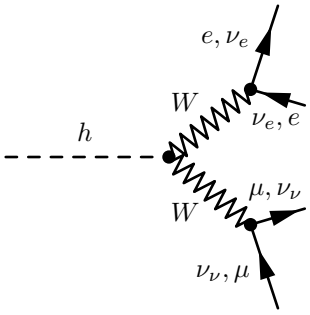

The signature for this channel is two opposite-charge leptons with large transverse momentum and a large momentum imbalance in the event due to the escaping neutrinos.

Analysis for the 8 TeV data is similar to the analysis for the 7 TeV data, but more stringent criteria are applied to reduce the background and some selections have been modified to mitigate the impact of the higher instantaneous luminosity at the LHC is 2012. The e/mu final state provides more than 85% of the sensitivity.[1]

A. Event Selection

For the 8 TeV data, events are selected based on single-muon and single-electron triggers, which both require a lepton with transverse momentum > 24 GeV. Cosmic-ray muons, noise in the calorimeters and non-collision backgrounds are suppressed via careful criteria restriction. The primary vertex selection is the same as that in section IV.

Candidates for this channel are selected by requiring exactly two oppositely charged leptons of different falvours, with transverse momentum thresholds of 25 GeV for the leading lepton and 15 GeV for the subleading lepton. The dilepton invariant mass is required to be greater than 10 GeV. [1]

Since two neutrinos are present in the final state, events are required to have a large "missing" transverse energy. This is the negative vector sum of the transverse momenta of the reconstructed objects, including muons, photons, jets, and clusters of calorimeter cells not associated with these objects. This vector is used to determine the direction of the neutrinos or other missing objects. [1]

B. Background Normalization

The leading backgrounds from SM processes producing two isolated high-transverse momentum leptons are WW and top (both tt and single top). These are estimated using partially data-driven techniques based on normalizing the MC predictions to the data in control regions dominated by the relevant background source. The control and validation regions are defined by selections similar to those used for the signal region, but with some criteria modified to obtain samples enriched to a particular background.[1]

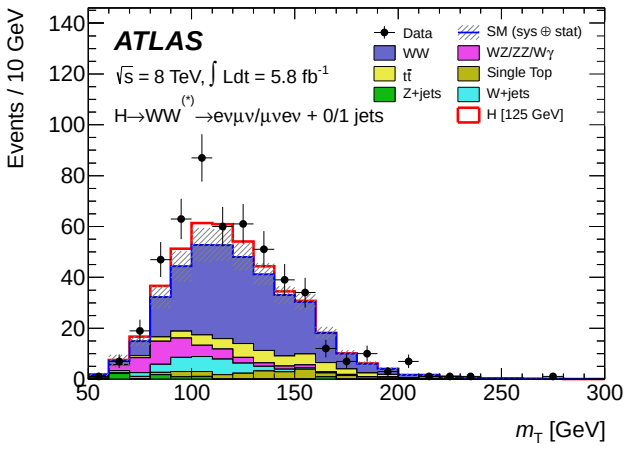

FIG. 4: Distribution of the transverse mass for both $e\mu$ and μe channels combined, for events satisfying all selection criteria

C. Systematic Uncertainties

The largest impact on the signal uncertainty originates from the theoretical uncertainties (refer to Section IX - Results). The main experimental uncertainties are associated with the jet energy scale (JES) and the jet energy resolution (JER) and luminosity. Other contributing factors are minor compared to these.[1]

A test beam with known particles of known energy is fired and measured in the calorimeter. This gives a reference for how much scintillation corresponds to a given amount of energy, which is then used as a reference for further jets.

There are a number of effects that spoil the accuracy of the conversion of light into a jet energy and the subsequent measurement of the originating quark energy. For instance, particles punch through the calorimeter without leaving all their energy inside, or they hit parts of the device which are "uninstrumented" or malfunctioning. The part of the calorimeter measuring the jet may be hit by additional particles not belonging to the jet originated from the quark, affecting the measurement. The deviation of the peak of the distribution from the true (modeled) value is the scale error [4].

D. Results

Fig. 4 shows the distribution of the transverse mass after all selection criteria in the 0-jet and 1-jet channels combined, and for both lepton channels together. An

excess of events relative to the background expectation is observed in the data.

The statistical analysis of the data employs a binned likelihood function (see section XI E. Binned Likelihood Analysis for details) constructed using the product of Poisson probability terms for the $e\mu$ and μe channels.

VII. STATISTICAL PROCEDURE

The RooStats Project is a project to create advanced statistical tools required for the analysis of LHC data, with emphasis on discoveries, confidence intervals, and combined measurements. The idea is to provide the major statistical techniques as a set of C++ classes with coherent interfaces, so that can be used on arbitrary model and datasets in a common way. [5]

All statistical methods require a probability density function and/or a likelihood function as input model. RooFit provides classes for facilitating the declaration of models and a way to re-use them in multiple statistical methods, since it has no statistical notion of parameters and observables. Therefore, it can work naturally with both frequentist and bayesian techniques. RooStats can then be considered as providing high-level statistical tools, while RooFit provides the core data modeling infrastructure [5].

These methods differ also in the way they incorporate the parameters for producing the results, so there is a need to have all of them.

VIII. CORRELATED SYSTEMATIC UNCERTAINTIES

The main sources of correlated systematic uncertainties are: integrated luminosity, electron and photon trigger identification, electron and photon energy scales, muon reconstruction, JES and missing transverse energy, and finally theoretical uncertainties.

The uncertainties, except for theoretical, are related to the calibration method, the resolution of the ID and MS, transverse momentum, transverse energy and η. The theoretical uncertainty mostly affect signal predictions. These are the QCD scale, predicted branching ratios, partition function distribution, signal normalization, and interference with other SM processes.

Sources of systematic uncertainty that affect both the 7 TeV and 8 TeV data are taken as fully correlated. The uncertainties on background estimates based on control samples in the data are considered uncorrelated between the 7 TeV and 8 TeV data. [1]

IX. RESULTS

The Standard Model does not predict the mass of the Higgs boson, but does predict the production cross section once the mass is known.

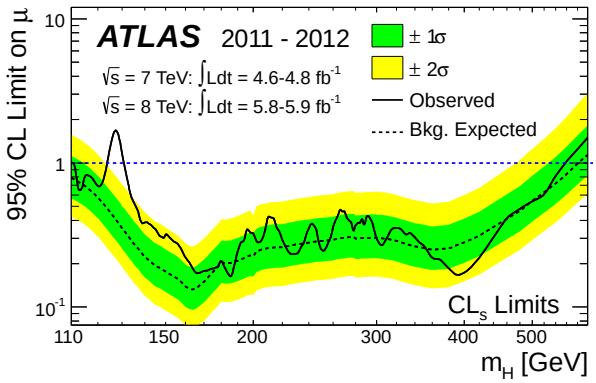

FIG. 5: Combined search results: The observed (solid) 95% CL upper limit on the signal strength as a function of the Higgs mass and the expectation (dashed) under the background-only hypothesis. The green and yellow bands show the $\pm 1\sigma$ and $\pm 2\sigma$ uncertainties on the background-only expectation.

For Fig. 5, the vertical axis shows, as a function of the Higgs mass, the Higgs boson production cross-section that is excluded, divided by the expected cross section for Higgs production in the Standard Model at that mass. This is indicated by the solid black line. This shows a 95% confidence level, which in effect means the certainty that a Higgs particle with the given mass does not exist. The dotted black line shows the median (average) expected limit in the absence of a Higgs. The green and yellow bands indicate the corresponding 68% and 95% certainty of those values. [1]

A. Excluded Mass Regions

In Fig. 5, if the solid black line dips below the value of 1.0 as indicated by the red line, then the data shows that the Higgs boson is not produced with the expected cross section for that mass. This means that those values of a possible Higgs mass are excluded with a 95% certainty. If the solid black line is above 1.0 and also somewhat above the dotted black line (an excess), then there might be a hint that the Higgs exists with a mass at that value. If the solid black line is at the upper edge of the yellow band, then there may be 95% certainty that this is above the expectations. It could be a hint for a Higgs boson of that mass, or it could be a sign of background processes or of systematic errors that are not well understood. [1]

B. Observation of an Excess of Events

The observation of more of a certain type of event than expected in a data plot is called an excess. The statistical significance of excesses determines how certain a result is

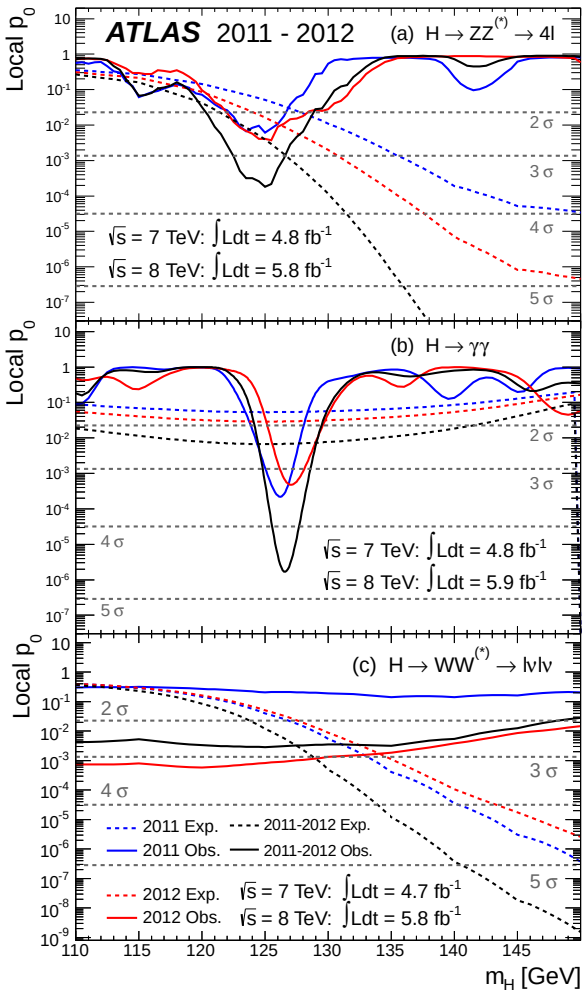

FIG. 6: The observed local p_0 as a function of the hypothesized Higgs boson mass for the (a) $H \to ZZ^{(*)} \to 4l$, (b) $H \to \gamma\gamma$ and (c)$H \to WW^{(*)} \to e\nu_e\mu\nu_\mu$ channels. The dashed curves show the expected local p_0 under the hypothesis of a SM Higgs boson signal at that mass. Results are shown separately for the 7 TeV data (dark, blue), the 8 TeV data (light, red), and their combination (black).

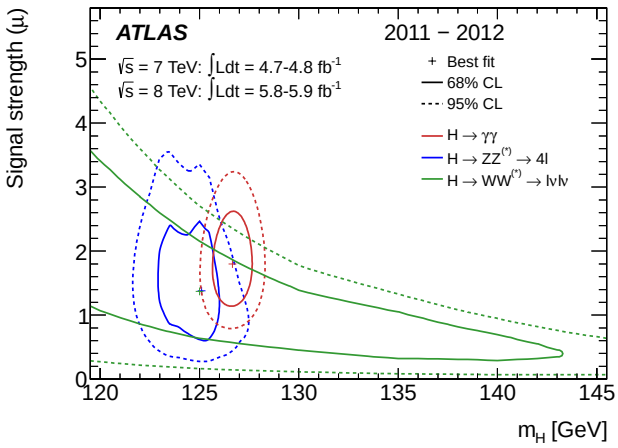

FIG. 7: Confidence intervals in the (μ, m_H) plane for the $H \to ZZ^{(*)} \to 4l$, $H \to \gamma\gamma$ and $H \to WW^{(*)} \to e\nu_e\mu\nu_\mu$ channels, including all systematic uncertainties. The markers indicate the maximum likelihood estimates $(\hat{\mu}, \hat{m_H})$ in the corresponding channels (the maximum likelihood estimates for $H \to ZZ^{(*)} \to 4l$ and $H \to WW^{(*)} \to e\nu_e\mu\nu_\mu$ coincide).

C. Characterizing the Excess

The mass of the observed new particle is estimated using the profile likelihood ratio for $H \to ZZ^{(*)} \to 4l$ and $H \to \gamma\gamma$, the two channels with the highest mass resolution as seen in Fig. 7. In order to test which values of the signal strength μ and mass of a signal hypothesis are simultaneously consistent with the data, the profile likelihood ratio $\lambda(\mu, m_H)$ is used. In the presence of a strong signal, it will produce more closed contours around the best fit point $(\hat{\mu}, \hat{m_H})$, while in the absence of a signal the contours will be upper limits on μ for all values of m_H.[1]

from new physics, and not simply random fluctuations.

As shown in Fig. 6s (a) and (b) , an excess of events is observed near $m_H = 126$ GeV in the $H \to ZZ^{(*)} \to 4l$ and $H \to \gamma\gamma$ channels, both of which provide fully reconstructed condidates with high resolution in invariant mass. These excesses are confirmed in the highly sensetive but low resolution $H \to WW^{(*)} \to e\nu_e\mu\nu_\mu$ channel as seen in Fig. 6 (c).

The largest local significance for the combination of the 7 and 8 TeV data is foudn for a SM Higgs boson mass hypothesis of $m_H = 126.5$ GeV, where it reaches 6σ. [1]

X. CONCLUSION

The Standard Model Higgs boson is excluded at 95% CL in the mass range 111-559 GeV, except for the narrow region 122-131 GeV. In this region, an excess of events with significance 5.9 σ is observed.

These results provide conclusive evidence for the discovery of a new particle with mass 126 $\pm$ 0.4(stat)$\pm$o.4(sys) GeV. The signal strength parameter μ has the value 1.4$\pm$0.3 at the fitted mass, which is consistent with the SM Higgs boson hypothesis. The decays to pairs of vector bosons whose net electric charge is zero identify the new particle as a neutral boson. The observation in the diphoton channel disfavours the spin-1 hypothesis. [1]

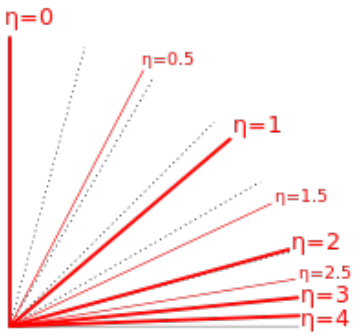

FIG. 8: Pseudorapidity values shown on a polar plot. In particle physics, an angle of zero is usually along the beam axis, and thus particles with high pseudorapidity values are generally lost, escaping through the space in the detector along with the beam.

XI. SUPPLEMENTARY

A. Pseudorapidity

Pseudorapidity, η, is a commonly used spatial coordinate describing the angle of a particle relative to the beam axis. It is defined as

$$\eta = -\ln\left[\tan\left(\frac{\theta}{2}\right)\right] \tag{1}$$

where θ is the angle between the particle three-momentum $\mathbf{p}$ and the positive direction of the beam axis.[6]

In hadron collider physics, pseudorapidity is preferred over the polar angle θ because differences in pseudorapidity are Lorentz invariant along the longitudinal axis.[6]

$$\eta' = -\ln\left[\tan\left(\frac{\theta}{2}\right)\right] - \ln(\gamma) \tag{2}$$

$$\Rightarrow \eta_1 - \eta_2 = \eta_1' = \eta_2'. \tag{3}$$

This is useful because in hadron collisions, it's often the case that one of the individual quarks or gluons involved in the collision may have a lot more momentum than the other, so all the particles produced come out near one end of the detector. But by translating the graph appropriately, it is possible to effectively shift to the center-of-mass frame of the colliding quarks or gluons, where the particles come out symmetrically distributed, and is therefore easier to analyze.

Notice that

$$\left|\frac{d\eta}{d\theta}\right|_{\theta=\frac{\pi}{2}} = 1, \tag{4}$$

since the resolution is best at $\theta = \pi/2$. So in particular, a circular jet will appear circular on the graph. This requires that the two coordinates be scaled the same way.

B. Cross Section

Cross section σ refers to the probability that two particles will collide and react in a certain way. The proton-proton to top-antitop cross section countis how many top-antitop pairs were created when a given number of protons were fired at each other. Cross section is independent of the intensity and focus of the particle beams, so cross section numbers measured at one accelerator can be directly compared with numbers measured at another, regardless of how powerful the accelerators are.

For two particles colliding to form n particles:

$$\begin{aligned}\frac{d\sigma}{d\Omega} =& \frac{s\hbar^2}{4\sqrt{(p_1\cdot p_2)^2 - (m_1m_2c^2)^2}} \int |M|^2 \\ & (2\pi)^2\delta^4(p_1+p_2-p_3-p_4-\cdots-p_n) \\ & \prod_{j=3}^{n}(2\pi)\delta(p_j^2-m_j^2c^2)\theta(p_j^0)\frac{d^4p_j}{(2\pi)^4},\end{aligned} \tag{5}$$

where Ω is the angular span of the detector and M is the lorentz invariant matrix element.

C. Branching Ratio

The probability that a particle will decay into one channel as opposed to another is called the branching ratio R. It is defined as the ratio of the cross sections for the particular decay channels.

$$R = \frac{\sigma(channel1)}{\sigma(channel2)}. \tag{6}$$

Fig. 9 displays the relative branching ratios for the SM Higgs. Placing a vertical line at the Higgs mass gives the ratios for that mass. Note that at $m_h \approx 125$ GeV, the Higgs is most likely to decay to a bottom/anti-bottom pair.

Using the results from section XI G with $m_h = 125$, $M_W = 80$ and $M_Z = 91$,

$$\frac{\Gamma(WW)}{\Gamma(ZZ)} = 0.98 \tag{7}$$

D. Luminosity

Luminosity $\mathcal{L}$ is used as a proportionality factor between the cross section σ and the number of interactions per second $\frac{dR}{dt}$.

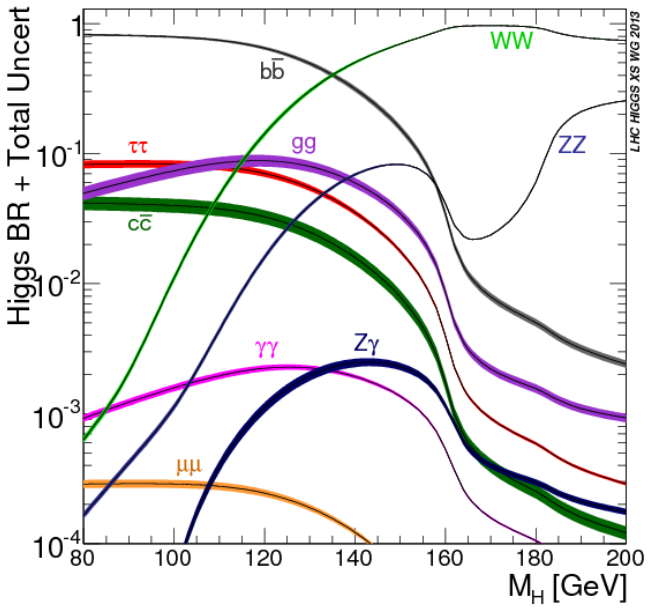

FIG. 9: Branching ratios of the SM Higgs.

$$\frac{dR}{dt} = \mathcal{L} \times \sigma \tag{8}$$

The luminosity is valuable, as it is relativistically invariant, independent of the physical reaction and is easy to compute and measure. In a collider, the target is the other beam, which is moving. Therefore, the collider luminosity per bunch crossing is examined. Complications arise in the form of the angle between the beams, non-Gaussian profiles and dispersion.

E. Binned Likelihood Analysis

When two different models, or perhaps two variants of the same model differing only in the value of some adjustable parameters, are to be compared as explanations for the same observed outcome, the probability of obtaining this particular outcome can be calculated for each and is then known as the likelihood for the model or parameter values given the data.

The Poisson distribution Eq. 9

$$p_i = \frac{\theta_i^{n_i} e^{-\theta_i}}{n_i!} \tag{9}$$

describes the probability of a number of events occurring in a given point, where n_i is number of observed counts at point i and θ. [7]

F. Lifetime of the Higgs

From FIG. 3, it is possible to estimate the lifetime of the Higgs boson. Using the time-energy uncertainty principle (Eqn. 10)

$$\Delta E \Delta t \geq \frac{\hbar}{2}, \tag{10}$$

and determination of the energy will characterize the time scale for a change in the system. In this case, ΔE results from the full width at half maximum (FWHM) in the " Σ weights or Events - Bkg" plots.

G. Decay Rates

For a theoretical approach to determining the lifetime of the Higgs boson, the matrix elements M and the decay rate Γ are determined from Feynman calculus. The lifetime is defined as the inverse of the decay rate.

For particle 1 decaying to n particles:

$$\begin{aligned}\Gamma =& \frac{S}{2\hbar m - 1} \int |M|^2 \\ & (2\pi)^2 \delta^4(p_1 + p_2 - p_3 - p_4 - \cdots - p_n) \\ & \prod_{j=3}^{n} (2\pi)\delta(p_j^2 - m_j^2 c^2)\theta(p_j^0) \frac{d^4 p_j}{(2\pi)^4}\end{aligned} \tag{11}$$

1. $h \to f\bar{f}$

Using a vertex factor of $\frac{imc^2}{v\sqrt{\hbar c}}$ [8],

$$M = i\left[\bar{v}(3)\left(\frac{imc^2}{v\sqrt{\hbar c}}\right)\right] u(2) \tag{12}$$

$$= -\frac{mc^2}{v\sqrt{\hbar c}} [\bar{v}(3)u(2)] \tag{13}$$

$$\Rightarrow |M|^2 = \left(\frac{mc^2}{v\sqrt{\hbar c}}\right)^2 Tr[(\not{p}_2 + mc)(\not{p}_3 - mc)] \tag{14}$$

$$= 4\left(\frac{mc^2}{v\sqrt{\hbar c}}\right)^2 [p_2 \cdot p_3 - (mc)^2] \tag{15}$$

In the CM frame,

$$|M|^2 = 8\left(\frac{mc^2}{v\sqrt{\hbar c}}\right)^2 \left[\left(\frac{E}{c}\right)^2 - (mc)^2\right]. \tag{16}$$

From conservation of energy,

$$|M|^2 = 8\left(\frac{mc^3}{v\sqrt{\hbar c}}\right)^2 \left(m_h^2 - 4m^2\right) \tag{17}$$

so that the decay rate Γ is

$$\Gamma(f\bar{f}) = \frac{1}{8\pi\hbar m_h^2}\left(\frac{mc^3}{v\sqrt{\hbar c}}\right)^2\left(m_h^2 - 4m^2\right)^{3/2}. \quad (18)$$

2. $h \to W^-W^+$ and $h \to ZZ$

Using a vertex factor of $2i\frac{M^2c^3}{c\sqrt{\hbar c}}g^{\mu\nu}$ [8] where M is the mass of W or Z,

$$M = i\epsilon_\mu^*(2)\left(i\frac{M^2c^3}{c\sqrt{\hbar c}}g^{\mu\nu}\right)\epsilon_\nu^*(3) \quad (19)$$

$$\Rightarrow |M|^2 = \left(\frac{2M^2c^3}{v\sqrt{\hbar c}}\right)^2\left[\epsilon_\mu^*(2)\epsilon^{*\mu}(3)\right]\left[\epsilon_\nu(2)\epsilon^\nu(3)\right] \quad (20)$$

Summing over the outgoing spins [8],

$$\left\langle|M|^2\right\rangle = \left(\frac{2M^2c^3}{v\sqrt{\hbar c}}\right)^2\left[-g_{\mu\nu} + \frac{p_{2\mu}p_{2\nu}}{(Mc)^2}\right]\left[-g^{\mu\nu} + \frac{p_3^\mu p_3^\nu}{(Mc)^2}\right] \quad (21)$$

$$\Rightarrow \left\langle|M|^2\right\rangle = \left(\frac{2c}{v\sqrt{\hbar c}}\right)^2\left[2(Mc)^4 + (p_2\cdot p_3)^2\right] \quad (22)$$

In the CM frame,

$$\left\langle|M|^2\right\rangle = \left(\frac{c^3}{v\sqrt{\hbar c}}\right)^2\left(m_h^4 - 4m_h^2M^2 + 12M^4\right) \quad (23)$$

Then, the decay rate is

$$\Gamma(WWorZZ) = S\frac{m_h^3c^5}{16\pi\hbar^2v^2}\left(\frac{c^3}{v\sqrt{\hbar c}}\right)^2\left(m_h^4 - 4m_h^2M^2 + 12M^4\right) \quad (24)$$

with $S = 1$ for WW and $S = 1/2$ for ZZ.

[1] ATLAS Collaboration *Observation of a new particle in the search for the Standard Model Higgs boson with the ATLAS detector at the LHC*, Physics Letters B. Volume 716, Issue 1, 17 September 2012, Pages 129

[2] The Detector — ATLAS. (n.d.). Retrieved March 26, 2016, from http://atlas.cern/discover/detector

[3] B. Webber, *Monte Carlo Methods in Particle Physics*, University of Cambridge 2007.

[4] S. D. Ellis, D. E. Soper, *Successive Combination Jet Algorithm For Hadron Collisions*, Phys. Rev. D48, 31603166 (1993)

[5] L. Moneta, K. Belasco, K. S. Cranmer, S. Kreiss, A. Lazz aro, et al., *The RooStats Project* , PoS ACAT2010 (2010) 05

[6] Cheuk-Yin Wong *Introduction to High-Energy Heavy-Ion Collisions*, (World Scientific, 1994)

[7] Canadas del Rio, Beatriz *Introduction to Binned Likelihood Analysis* (Multidark School on Fermi Tools, April 2010)

[8] David Griffiths *Introduction to Elementary Particles (2ed, revised)*, Wiley-VCH (2008)